Soft Matter

Capillary droplet propulsion on a fibre

Journal:	*Soft Matter*
Manuscript ID:	SM-ART-05-2015-001228.R1
Article Type:	Paper
Date Submitted by the Author:	22-Jun-2015
Complete List of Authors:	Haefner, Sabrina; University of Saarland, Department of Experimental Physics Baeumchen, Oliver; Max Planck Institute for Dynamics and Self-Organization, Jacobs, Karin; University of Saarland, Department of Experimental Physics

SCHOLARONE™
Manuscripts

ARTICLE TYPE www. rsc.org/xxxxxx | XXXXXXXX

Capillary droplet propulsion on a fibre

Sabrina Haefner,[a] Oliver Bäumchen[b] and Karin Jacobs*[a]

Received Xth XXXXXXXXXX 20XX, Accepted Xth XXXXXXXXX 20XX
First published on the web Xth XXXXXXXXXX 200X
DOI: 10.1039/b000000x

A viscous liquid film coating a fibre becomes unstable and decays into droplets due to the Rayleigh-Plateau instability (RPI). Here, we report on the generation of uniform droplets on a hydrophobized fibre by taking advantage of this effect. In the late stages of liquid column breakup, a three-phase contact line can be formed at one side of the droplet by spontaneous rupture of the thinning film. The resulting capillary imbalance leads to droplet propulsion along the fibre. We study the dynamics and the dewetting speed of the droplet as a function of molecular weight as well as temperature and compare to a force balance model based on purely viscous dissipation.

1 Introduction

Regular droplet patterns on a fibre are a well-known phenomenon, which can be found in everyday life, e.g. dew drops on a spider's web[1]. Thereby, small drops are pinned on the web filament, whereas big droplets are affected by gravitational flow and eventually coalesce with others. The destabilization and the subsequent breakup into uniform droplets of a liquid film on a fibre is caused - like in a free liquid jet - by the Rayleigh-Plateau instability[2,3] (RPI). Although, this is an obstructive effect in coating techniques, the capability to form regular droplets with an adjustable size and the control of their motion are very advantageous and important for technical applications e.g. water collection processes[4–6], patterning[7], chemical reactions[8] and printing[9]. The instability of liquid threads and its characteristics have been studied intensively over the last two centuries and is still of great interest[3,10–13]. Furthermore, many studies investigated the motion of beads flowing down a vertical fibre, sliding or rolling on a fibre or the mechanisms of droplet movement in filament networks[14–20]. However, only a few studies identify the motion of droplets in the absence of gravitational forces, where droplets are propelled along a fibre or on a planar substrate by taking advantage of different effects. For example, Yarin et al. studied the movement of drops along a cylindrical filament due to a temperature gradient[21], yet also a difference in pressure can lead to a propelling force[22]. Remarkably, liquid droplets can even detect and move along stiffness gradients of an underlying substrate (durotaxis)[23]. Another well-established and commonly used way of producing and transporting equally sized droplets on the micro scale is realized by using microfluidic devices, where droplets are generated and transported inside a channel[24].

Here, we report on viscous liquid droplets moving along the outer surface of a hydrophobized solid fibre, purely driven by capillary forces. For that purpose, droplets are generated by taking advantage of the RPI: In the course of the destabilization of a thin homogeneous film, liquid droplets separated by valleys are emerging. By spontaneous rupture of the thinning liquid film in between the equally distributed droplets, an axisymmetric three-phase contact line can be formed at one side of the droplet at the late stages of liquid column breakup. This leads to a capillary imbalance between the two ends of the droplet, which causes the drop to dewet on the fibre. Figure 1b shows a typical example of a receding polystyrene (PS) droplet on a hydrophobized glass fibre (see Supplementary Video V1). The motion process is studied as a function of molecular weight and temperature and is compared to the classical case of a dewetting ridge on a substrate.

2 Experimental

Glass fibres were prepared by pulling heated glass capillary tubes (World Precision Inst.) to final diameters of 20 to 30 μm using a pipette puller (Narishige, PN30). By dip-coating the glass fibres in a 0.5 wt% solution of AF2400 (Poly[4,5-difluoro-2,2-bis(trifluoromethyl)-1,3-dioxole-co-tertrafluoroethylene]) (Aldrich) in a perfluorocompound solvent (FC72^{TM}, Fisher Scientific), a hydrophobic amorphous fluoropolymer layer ($T_g \sim 240\,^\circ$C) is deposited on the fibres. In order to remove excess solvent, fibres were annealed to 80 °C for 90 minutes in ambient atmosphere.

To create droplets on a fibre, we apply a homogeneous polystyrene (PS) film with thickness e_0 (5 to 90 μm) onto the hydrophobized fibre (see Fig. 1a): Atactic polystyrene (Poly-

[a] *Saarland University, Department of Experimental Physics, 66041 Saarbrücken, Germany. E-mail: k.jacobs@physik.uni-saarland.de*
[b] *Max Planck Institute for Dynamics and Self-Organization (MPIDS), 37077 Göttingen, Germany.*

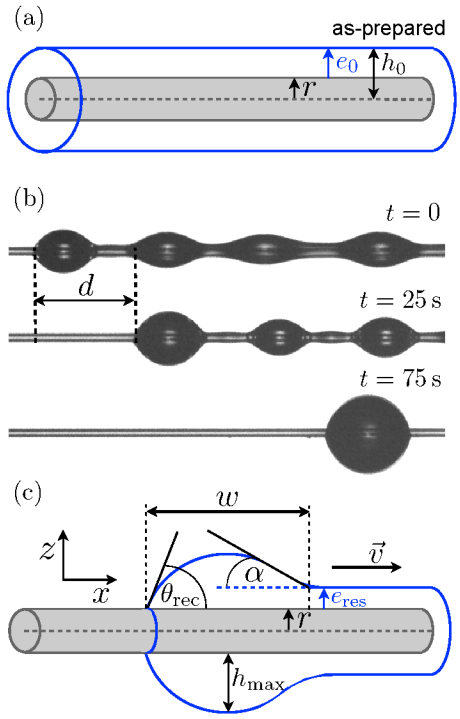

Fig. 1 (a) Schematic representation of the as-prepared samples: A homogeneous PS film with thickness e_0 is applied to a hydrophobized fibre with radius r. (b) Optical micrographs illustrating the time evolution of a polystyrene ($M_w = 8.1\,\mathrm{kg/mol}$) droplet receding on a hydrophobized fibre at a temperature of $T = 150^\circ\mathrm{C}$. The regular droplet pattern at $t = 0$ is achieved by utilizing the breakup of a homogeneous film on a cylindrical fibre into droplets, which are separated by a thin film. The spontaneous formation of a three-phase contact line at the left side of the far left droplet leads to a capillary imbalance, which causes the droplet to move to the right along the fibre. After a certain time t, the droplet has covered a particular distance d, while accumulating the residual thin film and static droplets. The width of the optical images is $1120\,\mu\mathrm{m}$. (c) Schematic representation of a droplet on a fibre during the motion process. All system geometries and parameters are indicated.

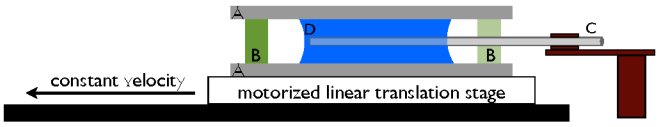

Fig. 2 Schematic representation of the PS film application setup (not to scale): A droplet of a highly viscous PS solution (D) is placed on a hydrophobized fibre (C), which is positioned close above a glass slide (A). Covering the system with a second glass slide on top of two Si-spacers (B) leads to the formation of a meniscus at the edges. The fibre (C) is located in the center of the PS droplet (D). By using a motorized linear translation stage, the PS solution is pulled along the fibre with a constant velocity, which results in the formation of a homogenous PS film with thickness e_0 surrounding the axisymmetric fibre.

mer Source Inc.) with molecular weights varying between 4.1 and 78 kg/mol and low polydispersities ($M_w/M_n = 1.05$) was dissolved in chloroform (Fisher Scientific). A droplet of a highly viscous (35 wt%) polymer solution was placed onto a hydrophobized fibre, which was positioned close above a glass slide (see Fig. 2). Covering the system with a second glass slide on top of two Si-spacers leads to the formation of a meniscus at the edges. By using a motorized linear translation stage (Newport), the PS solution is pulled along the fibre with a constant velocity, which results in the formation of a homogeneous PS film with thickness e_0 surrounding the axisymmetric fibre. By varying the speed between 80 and 120 mm/s films with thicknesses e_0 of 5 to $90\,\mu\mathrm{m}$ could be generated after solvent evaporation. All samples were prepared at room temperature, which is well below the glass transition temperature T_g of all used molecular weights[25,26].

In order to initiate the formation of droplets on a fibre, the as-prepared samples (see Fig. 1a) were annealed above T_g in ambient conditions. By placing the fibres across two 0.5 mm thick spacers, which are located on top of a reflective Si wafer, we achieve free standing filaments. This setup was positioned on a microscope hot stage (Linkam), while surrounded by a metal ring in direct contact with the hot stage. Finally, the metal ring is covered by a glass slide. Thereby, good thermal contact and temperature control within 1 K was ensured. As a result of annealing above the glass transition temperature, the liquid films became unstable and were subjected to the Rayleigh-Plateau instability[13]. Axisymmetric barrel shape[27,28] droplets with a certain spacing were formed. As the droplet size is related to the film thickness e_0 and the fibre radius r, the typical droplet height $h_{\mathrm{max}}(t)$ (see Fig. 1c) is in the range of 40 to $200\,\mu\mathrm{m}$. The width $w(t)$ of the droplets (see Fig. 1c) varies between 100 and $320\,\mu\mathrm{m}$. The fact that films below $e_0 = 5\,\mu\mathrm{m}$ start to dewet prior to the formation of droplets on a hydrophobized fibre implies that by using this technique of droplet generation, the lowest limit of possible droplet sizes has already been reached.

The thin liquid film in between the droplets represents a metastable situation, as can be concluded from the shape of the effective interface potential which comprises short-range and long-range interactions[29,30]. Any chemical or topographical heterogeneity can act as a nucleus leading to the formation of a hole in the film. This random process causes the axisymmetric rupture of the film and thus the formation of a three-phase contact line at one side of a droplet. Consequently, at this side of the droplet the contact angle is adapted to the receding contact angle θ_{rec} (see Fig. 1c). On the opposite side, however, where the droplet merges into the residual PS film, the apparent angle α remains constant. This causes the Laplace

This journal is © The Royal Society of Chemistry [year]

pressure to be different on both sides of the droplet and the capillary imbalance leads to droplet propulsion along the fibre. During droplet motion the residual material (thin film and static droplets) is accumulated. Thereby, the total volume of the system is conserved and the droplet grows in size. Typically, the height of the droplet $h_{\max}(t)$ increases by a factor of 1.5 to 2 and the width $w(t)$ grows by a factor of 1.2 to 1.7 over the entire dewetting process. As long as one side of the moving droplet is connected to the residual material, the capillary force on the ‚wet' side is negative and the three-phase contact line recedes. Thus, the droplet accumulates all the remaining material until the dewetting process finally results in the formation of isolated droplets sitting on the fibre (see Fig. 1b, $t = 75\,\mathrm{s}$). In this final configuration, the droplet has two 'dry' sides and the motion of the droplet stops as soon as both contact angles adapt to the equilibrium contact angle θ_e. The receding and the equilibrium contact angle, θ_{rec} and θ_e, of PS on an AF2400 fibre were determined from optical micrographs by using an image analysis software (Image Pro Plus, Media Cybernetics). Note that θ_{rec} has been evaluated during the accumulation of residual thin film e_{res} only (see Fig. 1c). Here, we measured $\theta_{rec} = 60 \pm 5^\circ$ and $\theta_e = 83 \pm 5^\circ$. The ratio between these two angles is in good agreement with studies on polymer films dewetting on planar hydrophobized surfaces[31–33], which showed a fixed relation of $\theta_e/\theta_{rec} \approx \sqrt{2}$. To determine the PS film thickness e_0, the initial total radius of the coated fibre h_0 was measured by optical microscopy with an accuracy of $\pm 1\,\mu\mathrm{m}$ (see Fig. 1a). The fibre radius r was measured (with an accuracy of $\pm 1\,\mu\mathrm{m}$) after the PS film dewetted (see Fig. 1b, $t = 75\,\mathrm{s}$). From their difference $e_0 = h_0 - r$, we achieve e_0. The motion of the droplet was recorded with optical microscopy. Figure 1b shows a typical time evolution of a droplet receding on a hydrophobized fibre (also see Supplementary Video V1). A custom made edge detection software in MATLAB is applied in order to record the travelled distance d (see Fig. 1b), i.e. the distance moved by the three-phase contact line of the droplet in a certain time t.

3 Results and discussion

This section incorporates the results of the experiments described above, followed by a comparison to a model based on a balance of capillary driving force and dissipation through viscous friction. In Section 3.1, we focus on the global dewetting process of a droplet on a fibre for various molecular weights and temperatures. Thereby, we identify the global dewetting velocity $\bar{v}$ including both processes, the accumulation of the residual thin PS film as well as the coalescence with remaining static droplets. Section 3.2 comprises a more local analysis of the dewetting behavior. We investigate the two different dewetting processes in more detail and determine the local velocity v as a function of molecular weight and temperature

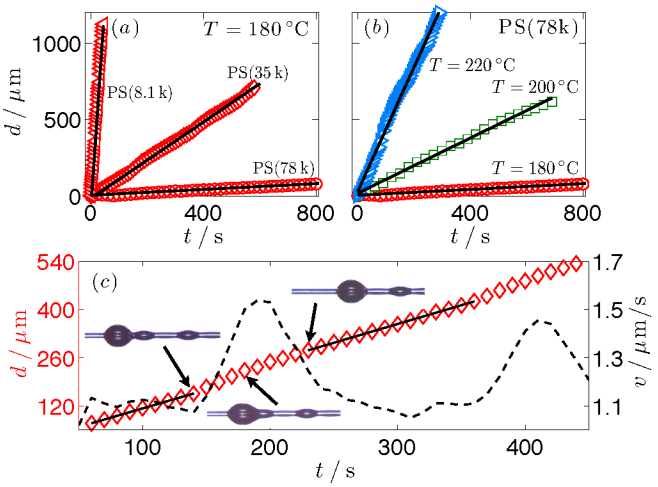

Fig. 3 Position d of the three-phase contact line on the fibre axis x as a function of time t for (a) different PS molecular weights at $T = 180°\mathrm{C}$ and (b) PS(78k) at different temperatures T. The black lines indicate the best linear fit for each data set. (c) Symbols indicate the travelled distance d as a function of time for a PS(35k) droplet at $T = 180°\mathrm{C}$ during the different steps of the dewetting process. The black dashed line displays the respective local speed v obtained by using the Savitzky-Golay[36] algorithm (here: $n = 7$, $p = 2$). The black straight lines indicate the best linear fit excluding coalescence steps.

neglecting coalescence steps. A description of the model and a comparison with experimental data is given in Section 3.3.

3.1 Global droplet dynamics

From the experimental images (see Fig. 1b) we measure the distance d, which gives the distance the three-phase contact line of the droplet has moved along the fibre axis x during a certain time interval. Fig. 3a displays typical data for different molecular weights using a constant temperature of $T = 180°\mathrm{C}$. In analogy, Fig. 3b shows a variation in temperature for a constant molecular weight of $M_w = 78\,\mathrm{kg/mol}$. We find that for all data sets the motion of the dewetting droplet is linear in time (linear fits in Fig. 3a, b) over the entire process. Thus, the slope of these curves provides a reliable measurement of the global mean droplet velocity $\bar{v}$. Fig. 3a shows that for a constant annealing temperature T, the global mean velocity of a moving droplet is increasing when decreasing the molecular weight M_w, which is accompanied by a decrease in the viscosity η[34,35]. This observation is entirely consistent with Fig. 3b, where for a constant molecular weight we observe an increase in the global mean speed with increasing the temperature, again equivalent to a decrease in η. Furthermore, the linearity in the mean velocity during the entire motion (see Fig. 3a, b) indicates that there is no influence of the increase

in the height $h_{\max}(t)$ and width $w(t)$ of the droplet (due to material accumulation) on the dewetting dynamics.

3.2 Local analysis of the droplet velocity

Having characterized the global droplet dynamics, we now turn to a more local analysis of the droplet velocity. Based on the algorithm by Savitzky and Golay[36], the local velocity v is calculated from the three-phase contact line displacement-time data. We chose a frame size of $n = 3$ and a second order polynomial ($p = 2$) for the interpolation of the experimental data. Figure 3c shows typical data of the travelled distance d as a function of time (symbols, see Fig. 3a). We found that the local velocity v of the droplet (dashed line) is alternating around the global mean velocity $\bar{v} = 1.2\,\mu$m/s: As the droplet dewets and accumulates the residual thin PS film, both, the receding contact angle θ_{rec} and the velocity v remain constant. As soon as the moving droplet gets in contact with one of the static droplets on the fibre, a sudden increase of the driving force due to the pressure gradient between the droplets is observed. The neck in between the two droplets levels rapidly, which causes the dewetting velocity v to increase (see Fig. 3c) and consequently the contact angle θ_{rec} to decrease. At the end of the coalescence process, the droplet shape recuperates, which goes in line with a deceleration of the speed and the adjustment of the receding contact angle. Thus, for simplicity, we consider in the following only the local velocity of a droplet during the consumption of the residual thin film, referred to as v. Accordingly, the coalescence steps with immobile droplets are neglected for the purpose of determining the droplet velocity v. The solid black lines in Fig. 3c show the linear best fit to the respective sections of the data. The local velocity turns out to be consistent for different sections of the data. Thus, there is no evidence for the local velocity v to be systematically affected by the change of the droplet size. Fig. 4 represents typical data for the local velocity as a function of the initial system radius h_0 for three different viscosities ($M_{\text{w}} = 78$ kg/mol, $T = 180\,^{\circ}$C, $200\,^{\circ}$C, $220\,^{\circ}$C). The solid lines display the local mean dewetting speed averaged over the respective experiments. We see that varying the initial system radius h_0 (by varying the PS film thickness e_0 and the fibre radius r), which is directly linked with the size of the droplets, does not cause a significant change in the velocity.

3.3 Model

The mathematical description of a dewetting wedge-shaped liquid front has been addressed in previous studies[37,38]. The effective driving force per unit length F_{drive} of a dewetting liquid wedge (see Fig. 1c) is equal to the spreading parameter $|S|$. It denotes the energy difference per unit area between a dry substrate and a liquid covered surface and is

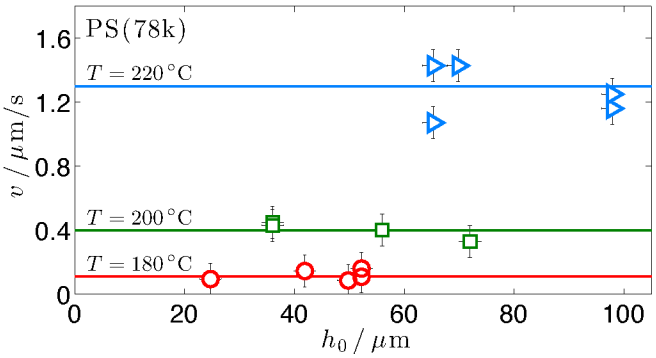

Fig. 4 Local velocity v of dewetting droplets on a fibre with a molecular weight of 78 kg/mol at different temperatures as a function of the initial system radius h_0. The straight lines indicate the local mean dewetting velocity for the different temperatures averaged over the respective experiments. The error bars are calculated from the error in the geometry and the error given by the dewetting velocity measurement.

given by $|S| = |\gamma_{\text{lv}}(\cos\theta_{\text{e}} - 1)|$, where $\gamma_{\text{lv}} = 30.8$ mN/m is the surface tension between the liquid (l) and the vapor (v) phase for polystyrene in air [*39]. Based on the work of Huh and Scriven[40], de Gennes developed a simplified model for the energy dissipation in a liquid wedge exhibiting a Poiseuille-type velocity profile $u(z)$, where the viscous dissipation power per unit length is described by:

$$D_{\text{visc}} = \int_0^{\infty}\int_0^{\zeta} \eta \left(\frac{du}{dz}\right)^2 dxdz = \int_0^{\infty} \frac{3\eta v^2}{\zeta} dx = \int_0^{\infty} \frac{3\eta v^2}{x\tan\theta_{\text{rec}}} dx, \tag{1}$$

with $\zeta = x\tan\theta_{\text{rec}}$ representing the local film height, η being the fluid viscosity and v standing for the velocity of the receding wedge. The divergence of the integral at both ends can be avoided by cutting the integral at the lateral position $x = w$ (which is an appropriate upper limit length scale like the width of the drop) and at the molecular size $x = a$ representing a lower limit, which leads to:

$$D_{\text{visc}} = \frac{3\eta l}{\tan\theta_{\text{rec}}} v^2, \tag{2}$$

where $l \equiv \ln(w/a)$ denotes a dimensionless coefficient. With the power balance $F_{\text{drive}} v = D_{\text{visc}}$, the velocity v of a dewetting wedge on a planar substrate is given by:

$$\frac{1}{v} = \frac{3l}{|S|\tan\theta_{\text{rec}}} \eta = A\eta. \tag{3}$$

* Note, that the surface tension of a polymer melt depends on temperature and molecular weight. Here, the variation in γ_{lv} is very small ($< 10\,\%$) and the mean value of $\gamma_{\text{lv=30.8}}$ mN/m is used. The error caused by using the averaged surface tension value is negligible compared to the uncertainty of the viscosity (as mentioned later in the text).

This journal is © The Royal Society of Chemistry [year]

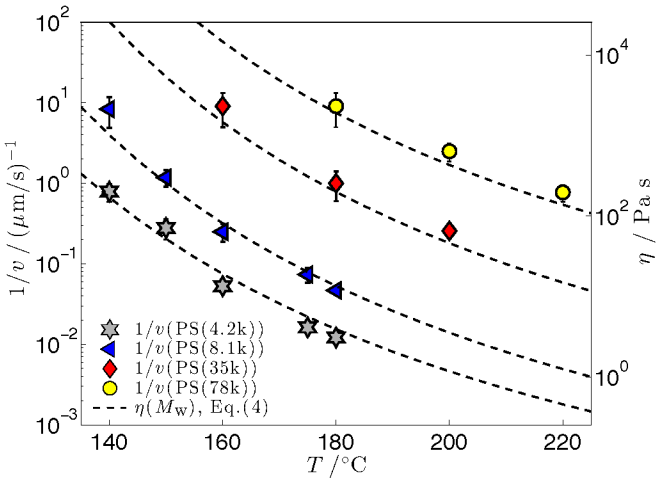

Fig. 5 Semilogarithmic representation of the inverse droplet velocity $1/v$ (symbols) and viscosity η according to Eq. (4) and independent viscosimeter measurements (dashed lines) for different molecular weights as a function of temperature T. The error bars represent the standard deviation of different dewetting velocity measurements. The inverse of the dewetting speed scales linearly with viscosity, exhibiting a universal constant of proportionality $A = 3900 \pm 300$ m/N.

This implies that in case of a purely viscous flow at the solid/liquid interface the velocity of a moving wedge is inversely proportional to the melt viscosity η, with $A = 3l/(|S| \tan\theta_{rec})$ representing the constant of proportionality.

Figure 5 shows a semi-logarithmic plot of the inverse local droplet velocity $1/v$ for various molecular weights ranging from 4.2 to 78 kg/mol as a function of temperature T (symbols). Typically, four to eight separate velocity measurements were averaged per data point. In addition, the respective viscosity data versus temperature is shown as dashed lines. The viscosities were determined from independent viscosimeter and ellipsometric measurements[33] by projecting the data according to the Williams-Landel-Ferry (WLF) equation[34,35]:

$$\eta = \eta_0 \exp\left(\frac{B}{f_0}\frac{T_g - T}{T - T_\infty}\right), \qquad (4)$$

where $\eta_0 = 6.3 \cdot 10^8$ Pa·s represents the viscosity at the glass transition temperature $T_g = T_g(\infty) - C/M_w$ for the respective M_w, with $T_g(\infty) = 372$ K and $C = 70$ K kg/mol for PS. The Vogel temperature is given by $T_\infty = T_g - 48$ K and the ratio $B/f_0 = 30.3$ is taken from literature[35].

In order to match the velocity data $1/v$ (symbols, left y-axis), the viscosities (dashed lines, right y-axis) are rescaled by a single constant prefactor A, which was found to be 3900 ± 300 m/N. This finding is consistent with experimental studies on dewetting holes in thin liquid polystyrene films with low molecular weights on hydrophobized flat surfaces[33].

Figure 6 displays the inverse of the measured local mean velocity $1/v$ as a function of viscosity η. The black line represents the linear scaling between $1/v$ and η with the universal proportionality constant A, as predicted by the force balance model based on purely viscous dissipation (Eq. (3)). Imposing the universal prefactor A as given above, this model turns out to be in good agreement with the experimental velocity data. Knowing the spreading parameter $|S|$ and θ_{rec} from the experimental data, the dimensionless coefficient l is the only free parameter. We obtain $l = 61 \pm 10$, which is in the same order of magnitude as in previous numerical studies[38], where l was found to range from 15 to 20. Experimental studies[31], e.g. on dewetting of PDMS on non-wettable surfaces by Redon et al. have reported a dimensionless coefficient of $l = 20$, whereas for more viscous alkanes $l = 6$ was obtained. A potential source of the deviation in l compared to other studies might originate from the fact that the polymer viscosity is very sensitive to variations in temperature and already a difference in T of 1 K can lead to a considerable systematic change in the dewetting dynamics. A second hypothesis is as follows: Dissipative particle dynamics simulations by Meriaba et al. did provide evidence that the viscous dissipation of a dewetting liquid front is predominantly located at the three-phase contact line[41]. Nevertheless, it is shown that viscous friction at the position, where the front merges into the residual thin film, represents a weak additional contribution to the dissipated energy. Assuming energy dissipation localized at both sides of the moving liquid front does not alter the scalings, Eq. (3), but justifies a decrease in the free parameter l[37,38]. In summary, we find that the model based on purely viscous dissipation captures the capillary-driven propulsion of axisymmetric droplets on hydrophobized fibres.

In the following paragraph, we will discuss friction at the solid/liquid interface, which has been identified as a potentially significant source of energy dissipation in thin film flows[32,33,42]: From an earlier study on the growth rates of amplitudes during the RPI it is known that PS(78k) on a hydrophobized fibre can exhibit significant hydrodynamic slip at the fibre/liquid interface[13]. The slip length b[43], which provides a quantitative measure for the amount of slip at the solid/liquid interface, was found to be $b = 4.0 \pm 0.4\,\mu$m for the exact same system. As the slip length scales with molecular weight[44,45], lower molecular weights are expected to exhibit a smaller slip length. Despite providing a slip boundary condition, which leads to a non-zero velocity of the polymer molecules at the solid/liquid interface[32,46], we find that the dynamics of a dewetting droplet is linear in time[32,33]. In addition, the local velocity v does not depend on the initial radius of the system h_0 (see Fig. 4) or rather the droplet size (height $h_{max}(t)$ and width $w(t)$), within the range of droplets sizes tested in our experiments. For smaller droplets one would expect to see an increase in the dewetting velocity as the PS

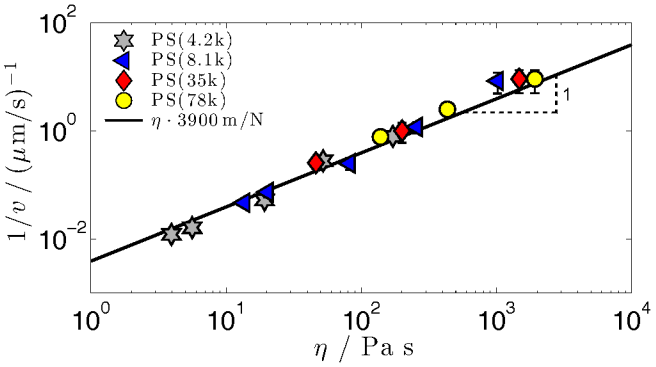

Fig. 6 Inverse droplet velocity $1/v$ as a function of viscosity η according to Eq. (4) and independent viscosimeter measurements. The error bars represent the standard deviation of different dewetting velocity measurements and do not include the uncertainty of the viscosity data taken from the WLF equation (see Eq. (4)). The black line represents the linear scaling between $1/v$ and η with the universal proportionality constant $A = 3900 \pm 300$ m/N.

film becomes sensitive to the enhanced mobility at the interface. By measuring the maximum droplet height $h_{\max}(t)$ (see Fig. 1c) we see that for all times t, the ratio between slip length b and maximal droplet height is equal to $b/h_{\max}(t) \leq 0.1$. This implies that the size of the droplets compared to b is too large to identify a considerable influence of the enhanced mobility at the solid/liquid interface on the dewetting speed. For large droplets, with $b/h_{\max}(t) \leq 0.1$, viscous friction at the contact line dominates over slippage. Thus, in our study, the dewetting dynamics is exclusively controlled by local dissipation at the contact line and the experimentally determined proportionality constant A, describing the linear scaling between $1/v$ and η, is universally valid (see Fig. 6).

4 Conclusions

Here, we have reported on the generation of uniform polystyrene droplets on a hydrophobized fibre by taking advantage of the Rayleigh-Plateau instability. Nucleation causes the spontaneous formation of a three-phase contact line at one side of a droplet. This leads to a capillary imbalance, which in turn causes the droplet to dewet on the fibre. Thereby, we found that the dynamics of a droplet is linear for all times and is as well geometry invariant. Considering the entire motion process including the accumulation of the residual thin film and the coalescence steps with static droplets shows that the dewetting velocity of the droplet is alternating around a certain mean velocity $\bar{v}$: The consumption of the thin polymer film features a constant droplet speed, but the coalescence process between moving and static droplets causes a local increase in velocity combined with a decrease in the receding contact angle. However, at the end of the merging procedure, θ_{rec} recovers and the speed is again decelerated. By neglecting the coalescence steps, the evaluation of the local droplet dynamics for varying molecular weights and temperatures exhibits a linear scaling between the inverse local dewetting velocity $1/v$ and viscosity η, consistent with the classical force balance model of a dewetting liquid wedge on a substrate based on purely viscous friction (see Eq. (3)). We found a single proportionality constant describing all data sets, which is in good agreement with former experimental studies on dewetting holes in thin films on hydrophobized surfaces[33]. Hence, we see that viscous dissipation dominates over slip-induced dissipation at the solid/liquid interface, for droplets which exhibit a height of at least ten times the corresponding slip length.

We expect these findings to be valid for all Newtonian liquids that are driven by capillarity and mediated by viscous forces. The precise control of droplet propulsion on microfibres might play an important role for practical applications and motivate novel designs of open microfluidic devices for chemical reactions and biological analysis. One might also envision new approaches and improvements in liquid deposition and patterning techniques. Finally, it provides a reliable and rapid method to determine the viscosity of a liquid.

5 Acknowledgement

The authors thank the graduate school GRK 1276, the German Research Foundation (DFG) under grant number BA3406/2 and NSERC of Canada. The authors also thank Kari Dalnoki-Veress, Thomas Salez, Michael Benzaquen, Elie Raphaël, Robert Peters and Joshua McGraw for fruitful discussions.

References

1 Y. Zheng, H. Bai, Z. Huang, X. Tian, F.-Q. Nie, Y. Zhao, J. Zhai and L. Jiang, *Nature*, 2010, **463,** 640-643.
2 J. Plateau in *Experimental and theoretical steady state of liquids subjected to nothing but molecular forces*, Gauthier-Villars, Paris, 1873.
3 F. Rayleigh, *Proc. London Math. Soc.*, 1878, **s1-10,** 4.
4 H. Bai, J. Ju, R. Sun, Y. Chen, Y. Zheng and L. Jiang, *Adv. Mater.*, 2011, **23,** 3708-3711.
5 J. Ju, H. Bai, Y. Zheng, T. Zhao, R. Fang and L. Jlang, *Nat. Commun.*, 2012, 3:1247 doi: 10.1038/ncomms2253.
6 K.-C. Park, S. S. Chhatre, S. Srinivasan, R. E. Cohen and G. H. McKinley, *Langmuir*, 2013, **29**, 13269-13277.
7 P. Ferraro, S. Coppola, S. Grilli, M. Paturzo and V. Vespini, *Nat. Nanotechnol.*, 2010, **5,** 429-435.
8 P. Azenbacher and M. A. Palacios, *Nat. Chem.*, 2009, **11,** 80-86.

This journal is © The Royal Society of Chemistry [year]

9 J.-U. Park, M. Hardy, S. J. Kang, K. Barton, K. Adair, D. K. Mukhopadhyay, C. Y. Lee, M. S. Strano, A. G. Alleyne, J. G. Georgiadis, P. M. Ferreira and J. A. Rogers, *Nat. Mater.*, 2007, **6,** 782-789.

10 S. L. Goren, *J. Colloid Interface Sci.*, 1964, **19,** 81-86.

11 R.-J. Roe, *J. Collid Interface Sci.*, 1975, **50,** 70-79.

12 J. Eggers, *Phys. Fluids*, 2014, **26,** 033106.

13 S. Haefner, M. Benzaquen, O. Bäumchen, T. Salez, R. Peters, J. McGraw, K. Jacobs, E. Raphaël and K. Dalnoki-Veress, *Nat. Commun.*, 2015, 6:7409 doi: 10.1038/ncomms8409.

14 D. Quéré, *Europhys. Lett.*, 1990, **13,** 721-726.

15 B. J. Mullins, I. E. Agranovski, R. D. Braddock and C. M. Ho, *J. Colloid Interface Sci.*, 2004, **269,** 449-458.

16 R. V. Craster and O. K. Matar, *J. Fluid Mech.*, 2006, **553,** 85-105.

17 T. Gilet, D. Terwagne and N. Vandewalle, *Appl. Phys. Lett.*, 2009, **95,** 014106.

18 T. Gilet, D. Terwagne and N. Vandewalle, *Eur. Phys. J. E*, 2010, **31,** 253-262.

19 R. Mead-Hunter, T. Bergen, T. Becker, R. A. O'Leary, G. Kasper and B. J. Mullins, *Langmuir*, 2012, **28,** 3483-3488.

20 F. Boulogne, L. Pauchard and F. Giorgiutti-Dauphiné, *J. Fluid. Mech.*, 2012, **704,** 232-250.

21 A. L. Yarin, W. Liu and D. H. Reneker, *J. Appl. Phys.*, 2002, **91,** 4751-4760.

22 E. Lorenceau and D. Quéré. *J. Fluid Mech.*, 2004, **510,** 29-45.

23 R. W. Style, Y. Che, S. J. Park, B. M. Weon, J. H. Je, C. Hyland, G. K. German, M. P. Power, L. A. Wilen, J. S. Wettlaufer and E. R. Dufresne, *Proc. Natl. Acad. Sci. U.S.A.*, 2013, **110,** 12541-12444.

24 R. Seemann, M. Brinkmann, T. Pfohl and S. Herminghaus, *Rep. Prog. Phys.*, 2012, **75,** 016601.

25 J. K. Keddie, R. A. Jones and R. A. Cory, *Europhys. Lett.*, 1994, **27,** 59-64.

26 S. Herminghaus, K. Jacobs and R. Seemann, *Eur. Phys. J. E*, 2001, **5,** 531-538.

27 G. McHale and M. I. Newton, *Colloids Surf., A*, 2002, **206,** 79-86.

28 H. B. Eral, J. de Ruiter, R. de Ruiter, J. M. Oh, C. Semprebon, M. Brinkmann and F. Mugele, *Soft Matter*, 2011, **7,** 5138.

29 R. Seemann, S. Herminghaus and K. Jacobs, *Phys. Rev. Lett.*, 2001, **86,** 5534-5537.

30 R. Seemann, S. Herminghaus and K. Jacobs, *Phys. Rev. Lett.*, 2001, **87,** 196101.

31 C. Redon, F. Brochard-Wyart and F. Rondelez, *Phys. Rev. Lett.*, 1991, **66**, 715-718.

32 R. Fetzer and K. Jacobs, *Langmuir*, 2007, **23,** 11617-11622.

33 O. Bäumchen, R. Fetzer, M. Klos, M. Lessel, L. Marquant, H. Hähl and K. Jacobs, *J. Phys.: Condens. Matter*, 2012, **24,** 325102.

34 M. L. Williams, R. F. Landel and J. D. Ferry, *J. Am. Chem. Soc.*, 1955, **77,** 3701-3707.

35 M. Rubinstein and R. H. Colby in *Polymer Physics*, Oxford Univ. Press. Inc., New York, 2003.

36 A. Savitzky and M. J. E. Golay, *Anal. Chem.*, 1964, **36,** 1627-1639.

37 P. G. de Gennes, *Rev. Mod. Phys.*, 1985, **57,** 827-863.

38 P. G. de Gennes, F. Brochard-Wyart and D. Quéré in *Capillarity and wetting phenomena: drops, bubbles, pearls, waves*, Springer-Verlag New York Inc., 2004.

39 J. Brandrup, E. H. Immergut and E. A. Grulke in *Polymer Handbook*, John Wiley & Sons Inc.: New York, 1999.

40 C. Huh and L. E. Scriven, *J. Colloid Interface Sci.*, 1971, **35**, 85-101.

41 S. Merabia and J. B. Avalos, *Phys. Rev. Lett.*, 2008, **101**, 208304.

42 O. Bäumchen and K. Jacobs, *J. Phys.: Condens. Matter*, 2010, **22,** 033102.

43 C. L. M. H. Navier, *Mem. Acad. Sci. Inst. Fr.*, 1823, **6,** 389.

44 P. G. de Gennes, *C. R. Acad. Sci. Ser. B*, 1979, 324.

45 O. Bäumchen, R. Fetzer and K. Jacobs, *Phys. Rev. Lett.*, 2009, **103,** 247801.

46 L. Bocquet and J.-L. Barrat, *Soft Matter*, 2007, **3,** 685-693.

Table of contents

We study the dewetting speed of polystyrene droplets on hydrophobized fibres as a function of molecular weight and temperature and compare to a force balance model based on purely viscous dissipation.